Focused on the "Portuguese contributions for Structural Integrity"

Visual Abstract

Algorithm for automatic fatigue crack growth simulation on welded high strength steels

R. Baptista
CDP2T, Department of Mechanical Engineering, ESTSetúbal, Instituto Politécnico de Setúbal, Campus do IPS, Estefanilha, 2914-761 Setúbal, Portugal
LAETA, IDMEC, Instituto Superior Técnico, Universidade de Lisboa, Av. Rovisco Pais, 1, 1049-001 Lisboa, Portugal
ricardo.baptista@estsetubal.ips.pt, https://orcid.org/0000-0002-5955-8418

J. Marques
Instituto Superior Técnico, ULisboa, Av. Rovisco Pais 1, 1049-001, Lisboa, Portugal
joao.p.ribeiro.marques@ist.utl.pt, http://orcid.org/0000-0003-0108-6363

V. Infante
LAETA, IDMEC, Instituto Superior Técnico, Universidade de Lisboa, Av. Rovisco Pais, 1, 1049-001 Lisboa, Portugal
virginia.infante@tecnico.ulisboa.pt, http://orcid.org/0000-0003-0860-2404

ABSTRACT. Nowadays the demand for high strength steels is increasing. In order to design and develop high performance products, it is essential to understand the fatigue behavior of these materials. When considering welded components, the fatigue behavior is even more complex. The material parameters may change along the crack growth and mixed mode crack propagation may also occur. To assess welded high strength steel fatigue behavior, different welded CT specimens were tested. The Paris law material constants were obtained for the heat affected zone material. Fatigue crack growth life predictions were made using the obtained parameters and different automatic techniques. Previous work showed that the ABAQUS extended finite element method can predict fatigue crack growth, but as the implementation of the Paris law is not straight forward, to many conversions must be made and the results are too computer intensive. A simpler and more intuitive Python algorithm was developed, to enable the use of the experimental material parameters, to predict the crack propagation path. The obtain results show a good agreement with both the experimental Paris curves, and the analytical solution.

KEYWORDS. Fatigue; Crack Propagation; Mixed Mode; Welded High Strength Steel.

OPEN ACCESS

Citation: Baptista, R., Marques, J., Infante, V., Algorithm for automatic fatigue crack growth simulation on welded high strength steels, Frattura ed Integrità Strutturale, 48 (2019) 257-268.

Received: 14.09.2018
Accepted: 29.10.2018
Published: 01.01.2019

Copyright: © 2019 This is an open access article under the terms of the CC-BY 4.0, which permits unrestricted use, distribution, and reproduction in any medium, provided the original author and source are credited.

INTRODUCTION

As the demand for high strength steels (HSS) increases, so does the necessity to assess the integrity of the various mechanical components produced with these materials. The two major goals are: increase the components fatigue life expectancy, and their safety.
Previously, the study and analyses were constantly made from laboratory experiments, which were lengthy, expensive and sometimes difficult to implement, due to several rules. Today, there are new materials and mechanical components appearing to a daily rhythm, which must be tested and certified to be available for the consumers. Inevitably, the engineers presented with systematic solutions, with higher precision, such as the Finite Element Method, making the whole process effective and efficient. However, some mechanical phenomena have always been difficult to model with the FEM, amongst which the study of cracks, stationary and especially its propagation. This particular study is necessary in order to predict the mechanical behavior of the equipment but also in order to increase its life expectancy.
When considering welded materials, the problem is even more complex, as Maier et al. [1], showed that the fatigue crack propagations properties are influenced by the material microstructure of the heat affected zone (HAZ). Qiang et al. [2] also showed that the mixed mode fatigue crack propagation of welded HSS is not clear, as the welded material actually has a better fatigue behavior justified by the more favorable microstructure.
This study intends to study the fatigue behavior of HSS welded specimens using a newly developed algorithm for fatigue crack propagation. This algorithm can use any type of Finite Element Method (FEM) model to automatically calculate the Stress Intensity Factor (SIF) on the crack front and use the Paris Law to predict the elapsed number of cycles for a constant crack increment. The crack propagation direction is predicted using the Maximum Tangential Stress criterion, using the same methodology as Ayatollahi et al. [3]. The algorithm also allows to use or determine the direct Paris Law material parameters, unlike the ABAQUS implementation of eXtended Finite Element Method (XFEM), which forces parameters conversions and is also a very computer intensive solution, with an advantage of not requiring the remeshing of the model, Singh et al. [4].

MATERIAL AND METHODS (JOÃO)

Materials

The high strength TMCP steel was supplied under the requirements of S700MC in EN 10149-2 specification [5]. Tab. 1 and 2 present the mechanical properties and chemical composition of the said steel, respectively.

σ_y (MPa)	σ_{UTS} (MPa)	A(%)
785	867	13.4

Table 1: Mechanical properties of the tested S700MC steel.

C (max %)	Si (max %)	Mn (max %)	Al (min%)	S (max %)	P (max %)	Nb* (max %)	Ti* (max %)	V* (max%)
0.12	0.25	2.10	0.015	0.010	0.020	0.09	0.15	0.20

*Sum of Nb, Ti and V ≤ 0.22 wt-%.

Table 2: Chemical composition of the tested S700MC steel.

Welding

Two steel plates (1000 mm long, 200 mm width, 8 mm thick) were welded together by MAG welding (Kemppi Promig 530 automatized system). The electrode was a filler wire that presented a approx. the same composition; shield gas was Mison 8 (Ar+8%-CO2+0.03%-NO). The weld groove was V-shaped with a 50º angle and two weld passes were executed. The Interpass temperature for each weld was T_{room} ~ 23 ºC. An interpass time of at least 40 min was required for complete cooling. Fig. 1 displays a schematic representation of the joint design and of welding sequence.

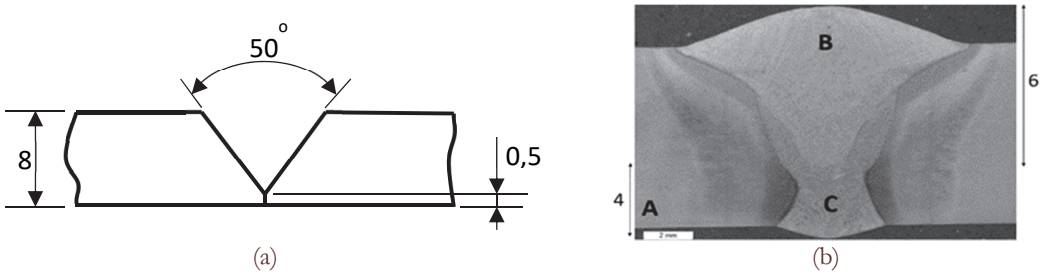

(a) (b)

Figure 1: Schematic representation of (a) joint design and (b) welding sequence (A: base metal; B: face pass; C: root pass) (dimensions in mm).

The applied heat input in each weld was determine using Eqn. (1) [6]. For the first pass the resulting t8/5 cooling time was 5 s while for the second pass was 10 s (Tab. 3).

$$t_{8/5} = \left(4300 - 4.3T_0\right) \cdot 10^5 \cdot \frac{k^2 \cdot Q^2}{t^2} \cdot \left[\left(\frac{1}{500 - T_0}\right)^2 - \left(\frac{1}{800 - T_0}\right)^2\right] \cdot F_2 \quad (1)$$

where T_0 represents the working temperature (in this case 23 ^{0}C), Q the heat input (kJ/mm), k is the thermal efficiency of the welding procedure (0.8 for the MAG welding case) and t is the workpiece thickness (8 mm). Finally, F_2 and is the joint type factor in two-dimensional heat conduction (0.9 in butt welds) [6].

Pass	$t_{8/5}$ (s)	Current (A)	Voltage (V)	Wire feed (m/min)	Travel speed (cm/min)	Heat input (kJ/mm)
root	5	253	25.8	11.7	55.7	0.7
face	10	270	28.6	12.7	46.3	1.0

$t_{8/5}$: cooling time from 800 °C to 500 °C.

Table 3. Welding parameters used.

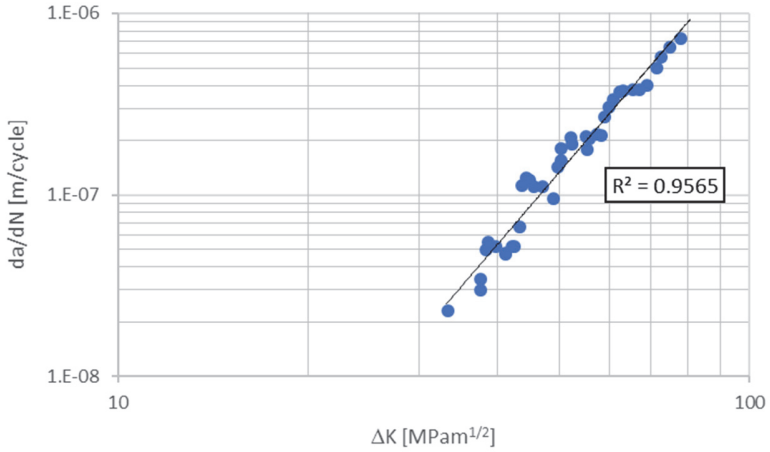

Figure 2: Paris Law data fit for the experimental results obtained on the heat affected zone.

Experimental Paris Law determination

Fatigue specimens were produced according to ASTM E466 96 [7]. Fatigue crack growth behavior was evaluated in the HAZ region at room temperature, according to ASTM E647 [8]. Fatigue tests were also carried out at room temperature with an MTS 810 servo hydraulic machine. The tests were performed under force-controlled mode using sinusoidal axial loading with constant amplitude. The stress ratio was 0.1 with *Pmax* = 10 kN, and *Pmin* = 1 kN. The load frequency was 5

Hz. A second derivative based Digital Image Correlation method (DIC) was used to measure the crack length evolution throughout the fatigue test (Lavision Imager Pro X camera system; speckle pattern produced with spray paint). Collected the crack length data, the Paris law was determine based on the seven point incremental polynomial technique presented in ASTM E 647 [8] (Fig. 2).

Algorithm for fatigue crack propagation

Previous work by the authors [9] showed that is possible to use closed FEM software's to calculate fatigue crack growth paths on complex geometries. Baptista et al. [9] have demonstrated that is possible to use ABAQUS XFEM module to calculate the Stress Intensity Factor (SIF) and automatically predict crack propagation direction and incrementation. Unfortunately, this commercial solution works as a black-box, therefore it is not possible to control the necessary parameters of crack propagation simulation procedure. In ABAQUS the user cannot input the experimentally determined Paris Law parameters. These must be converted, as ABAQUS uses the Paris Law in the Strain Energy Release Rate form. The process is also very computer intensive, and the final results can still be fine-tuned.

In order to solve the previously reported problems, several authors have developed alternative solutions, in order to calculate the fatigue crack growth path and fatigue life automatically. Dhondt [10] developed a solution using only freeware software. The algorithm used is common to other authors. First it is necessary to calculate the linear elastics fracture mechanics parameters for the different crack opening modes, for an initial crack. Next the Paris Law [11] is used to determine the crack propagation rate, and to predict the next crack increment. Finally, the crack can be updated, and the process is repeated. The algorithm developed by Dhondt [10] must therefore remesh the part in every increment. This method is more accurate but is also more computer intensive. As an alternative, other solutions have been developed. Rabold et al. [12] have developed a solution using ABAQUS and Python. ProCrack [12], uses a global mesh with a XFEM crack to calculate the crack displacements for each increment, and a sub-model of the crack front to calculate the linear elastics fracture mechanics parameters using the contour integral technique. Therefore, it is possible to model complex geometries, but there is no need for complex meshing procedures around the crack front, as only a simple material tube is modeled in the sub-model. Shi et al. [13], have solve the problem using only XFEM. There is no need to remesh the part, but in order to achieve the necessary quality for the SIF solution, the mesh in the crack propagation area must use an element size of as low as 0.3 mm. The obtained results from Shi et al. [13] were satisfactory, but the process is also very computer intensive [13].

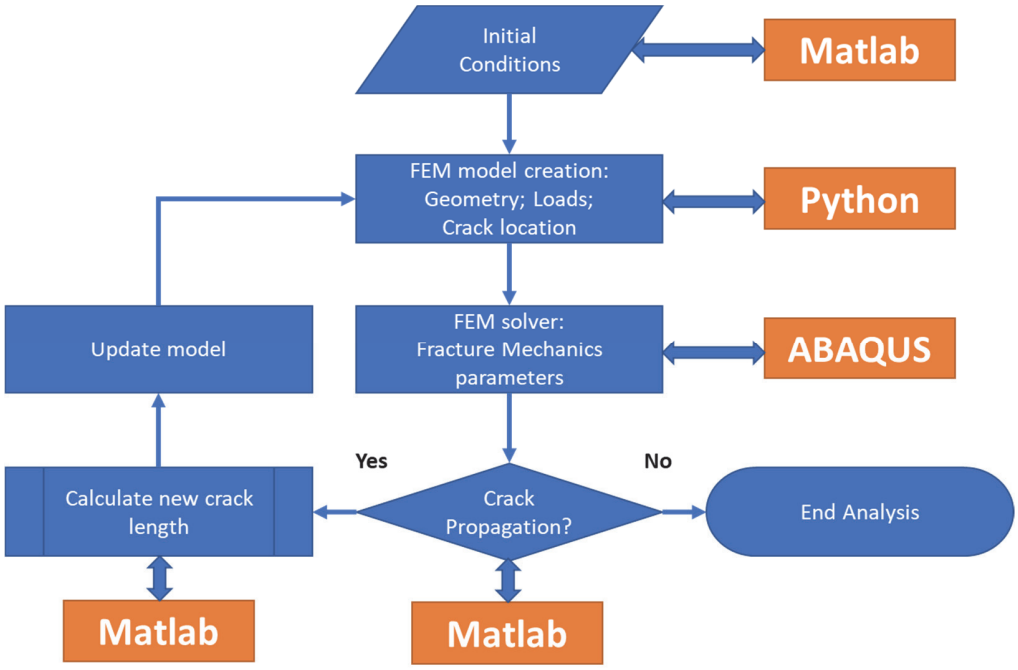

Figure 3: Flowchart of the algorithm used for fatigue crack growth simulation.

To avoid the problems encountered, the new algorithm developed in this paper does not use sub-models or constant meshes with high element densities. As proposed by Dhondt [10], requires part remeshing in each increment, but is not

limited to the contour integral technique, as it can also use the XFEM method. In this paper only ABAQUS was used as the FEM solver, but the algorithm can use any solver. This is possible because of the open and modular nature of the algorithm created. The main steps of the algorithm are represented in Fig. 3.
The initial conditions, the part geometry, the material properties and the loading conditions are initially set by a Matlab program. This program creates a Python script, using the necessary commands that the chosen FEM solver can recognize to create the FEM model. Python is therefore a translator that can create the FEM model in different FEM solvers. In our case the solver used was ABAQUS, that can calculate the SIF or other fracture mechanics parameters using different techniques. For two dimensional models ABAQUS can only use the contour integral technique, therefore a special mesh is required around the crack tip. Singular collapsed quadratic elements must be used, in a spider-web type mesh (Fig. 4). For three dimensional models ABAQUS can also use the XFEM technique to calculate the SIF. Our algorithm can create these three types of models, remeshing the part in each increment. For the contour integral models, a special spider-web mesh is created around the crack tip, Fig. 4, this mesh uses elements with a size of 0.1 mm, and 5 levels of elements are used of 5 SIF contours calculations. For XFEM models, the algorithm generates a square box, with a 1 mm side around the crack tip, filled with elements with a size of 0.05 mm. This is required to determine the SIF with the necessary quality, [13].

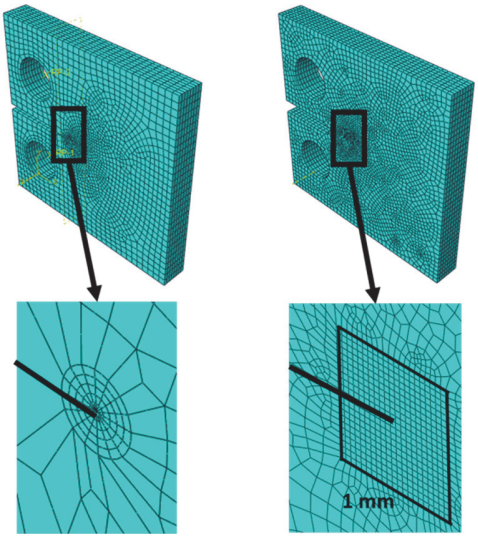

Figure 4: Special FEM mesh design around the crack front for the contour integral and XFEM techniques, used for SIF extraction.

ABAQUS returns the fracture mechanics parameters to Matlab, where the decision if the crack will propagate is made. This is the crucial step of the algorithm. If the crack can propagate, a new crack propagation direction must be calculated, and the crack driving force must be determined. Erdogan et al. [14] proposed the Maximum Tangential Stress (MTS) criterion for crack propagation in mode I. Several authors like Blažić et al. [15] or Fajdiga et al. [16], have successfully used the MTS criterion to calculate the fatigue crack growth direction in mode I and even in mixed mode conditions. According to Erdogan et al. [14] the new direction for the crack propagation, can be calculated using Eqn. (2).

$$\varphi = 2 \cdot tan^{-1}\left[\frac{1}{4}\left(\frac{K_I}{K_{II}} \pm \sqrt{\left(\frac{K_I}{K_{II}}\right)^2 + 8}\right)\right] \tag{2}$$

where φ is the new crack propagation direction, and K_I and K_{II} the SIF. While the crack driving force can be calculated by Eqn. (3).

$$\Delta K_{eq} = \frac{1}{4}\left(3cos\frac{\varphi}{2} + cos\frac{3\varphi}{2}\right)\Delta K_I - \frac{3}{4}\left(sin\frac{\varphi}{2} + sin\frac{3\varphi}{2}\right)\Delta K_{II} \tag{3}$$

Although these equations are valid in most cases, Yang et al. [17] have reported that some cracks show different behaviors in mixed modes. Some cracks opening mode will be governed by mode II and will behave according to the Maximum

Shear Stress (MSS) Criterion. Yu et al. [18] have compared the crack propagation in mode I and mode II, and proposed the basis for the implementation of the MTS and MSS criteria. Both have been implemented in the algorithm. The decision of which criteria to use is still very controversial. Yang et al. [17] mention that there is always a transition phase between the material behavior, where the MTS and MSS criteria are not applicable. While Zerres et al. [19] proposed a solution to calculate the crack driving force using a combination of both the MTS and MSS criteria. This might be a possible solution, but does not offer a determination of the crack propagation direction. By default, in the algorithm the MTS criterion is used. Finally, others authors have proposed different crack driving forces, as reviewed by Wang et al. [2] one of the most used, was given by Tanaka et al. [20] and can be represented by Eqn. (4). It is limited to be used with stress ratios higher than zero, when the crack will never be closed.

$$\Delta K_{eq} = \sqrt[4]{\Delta K_I^{\,4} + 8\Delta K_{II}^{\,4}} \tag{4}$$

Once the crack propagation direction and the crack driving force are determined, the next incrementation can be calculated. There are two possible routes, using a set crack length incrementation, and calculating the number of cycles for the increment, or using a set number of cycles, and calculating the corresponding crack length increment using Eqn. (5).

$$\Delta a = \Delta N \cdot \left(C \Delta K_{eq}^{\,m} \right) \tag{5}$$

Nasri et al. [21] have used a similar approach, using only the XFEM technique, and a set number of cycles between increments. This is a simple approach, but as mentioned by Shi et al. [13], this will lead to an accelerated crack propagation, and the final results will have poorer quality. Therefore the present algorithm uses a set value for the crack length increment, as used by Shi et al. [13], Lesiuk et al. [22] or Majid et al. [3]. According to the previous authors the crack length increment should be around 0.5 or 1 mm. The current algorithm can use smaller values for better results, but the computation time will increase. The algorithm can also determine the appropriate increment value, in an iterative process. But one can verify that the additional computation effort is not justified. Therefore, by default the user should choose the crack increment value for the analysis. The algorithm will finally update the model with the new crack front, and the procedure will be repeated, until a stopping condition is reached.

RESULTS AND DISCUSSION

In order to test and validate the developed algorithm, and to better understand the fatigue behavior of welded high strength steels, six FEM models were developed. Two 2D models, one representing a normal Compact Tension (CT) specimen and one representing a CT specimen containing a longitudinal weld. As the 2D specimens were modeled in plane strain, the welded specimen is only an approximation of the real geometry. Fig. 5 b) show a 3D representation of the developed 2D welded specimen, with different thickness on the welded area. Two 3D models, represented on Fig. 5 a) and c), of the normal and welded specimen. All four models used the contour integral technique to determine the SIF. Finally, two 3D models were also simulated using XFEM technique to extract the SIF values and to test the algorithm for crack propagation.

The SIF values were used to perform a mesh convergence study. Tab. 4 show the final values of mesh densities used in the simulations. When using the contour integral technique on the normal specimens it is possible to use a lower number of nodes per model. When modeling the longitudinal welded specimens, the mesh density must be higher to achieve convergence. When using the XFEM technique the chosen mesh density was equal, but the mesh generation technique resulted in a lower number of elements overall, for the welded specimen. As one can see, ABAQUS models does not allow the use of quadratic elements, when using the XFEM technique, therefore the overall number of nodes is lower. A free mesh technique was always used, to allow for automatic mesh creation at each increment.

All specimens were design in according to ASTM-E647, with a width (W) of 50 mm and a thickness (B) of 8 mm. The longitudinal weld, as a height of 2 mm and a width of 14 mm. The fixating pins were not modeled. One reference point, in the center of each specimen hole, was tied to the hole surface. Allowing for specimen rotation around the virtual pin. Periodic boundary conditions forced the vertical displacement of each pin to be symmetrical. The remaining degrees of freedom were blocked. The specimens were subjected to a vertical load with an amplitude of 9 kN and R=0.1.

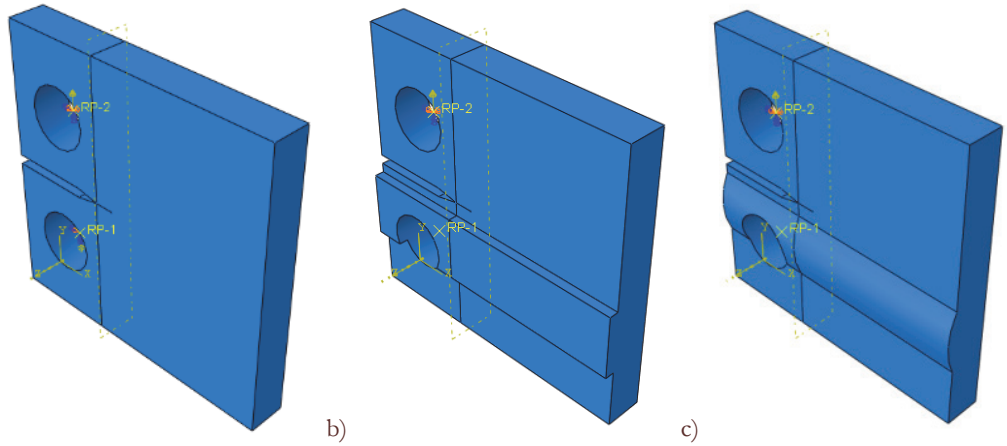

a) b) c)

Figure 5: Different CT specimens used in FEM simulations, a) normal 3D CT specimen (also simulated in 2D), b) 3D representation of the 2D simulated CT specimen containing a longitudinal weld, c) 3D CT specimen containing a longitudinal weld.

Specimen	Element Type	Nodes	Average element size [mm]	Element size near the crack front [mm]
Normal	2D Quadratic 8 nodes	14520	1.00	0.10
Longitudinal Weld	2D Quadratic 8 nodes	21300	0.75	0.10
Normal	3D Quadratic 20 nodes	68500	2.00	0.10
Longitudinal Weld	3D Quadratic 20 nodes	73400	1.50	0.10
Normal (XFEM)	3D Linear 8 nodes	40000	1.50	0.05
Longitudinal Weld (XFEM)	3D Linear 8 nodes	31600	1.50	0.05

Table 4: Element types and mesh densities used on FEM simulations.

Fatigue crack growth on a normal CT specimen

The modeled normal CT specimens were used to validate the algorithm predictions for pure mode I fatigue crack propagation. The algorithm accurately predicts the crack propagation direction, as all the cracks propagated in the horizontal direction. The periodic boundary conditions also guaranty that the value of the K_{II} is very close to zero, therefore there is no crack kinking tendency, as predicted by the MTS criterion in Eqn. (2). In order to compare the crack driving force, between models, one can use the results obtain with the ASTM-E647. As K_{II} is very close to zero, the crack driving force derived by Eqn. (3) or Eqn. (4) is equal to ΔK_I. Comparing the SIF obtained values with the ASTM-E647 results, one can see on Fig. 6, all the models predict a higher SIF. For cracks lengths inferior to 25 mm the difference increases as the crack length decreases. For crack lengths superior to 25 mm the differences remain constant. The 2D model maximum difference was 9% and for cracks lengths superior to 25 mm the difference is negligible. 3D models show higher differences, with the XFEM model resulting in a minimum difference of 4.5%, 1% higher than the contour integral model. This difference has also been reported by Shi et al. [13].

These differences are important when predicting fatigue life crack propagation using Eqn. (5). Higher SIF will predict a lower number of elapsed cycles for the same crack increment. As the algorithm uses a fixed value of crack increment the 3D models will underestimate the fatigue crack propagation life if one uses the same material properties. Therefore, to accurately predict crack propagation, using different models the Paris law material constants must be corrected for the appropriate model. Using the same methodology as in ASTM-E647, but the SIF values obtained for each model (Fig. 6), the Paris Law parameters were calculated for the different models. As the predicted SIF increases, the C parameter decreases, and the m parameter increases, Tab. 5. The XFEM model predicted a 4.5% higher SIF, resulting in a 32% lower C parameter and a 2% higher m parameter. While for the 2D contour integral model, where the differences between the SIF and the ASTM-E647 standard were lower, the C parameter resulted in a 16% lower value.

Fig. 7 shows a good agreement between all the models, the ASTM-E647 standard and the experimental results, for the crack propagating curve. This validates the algorithm and show that this approach, very similar to the one used by Zong et al. [23], is useful to predict fatigue crack propagation.

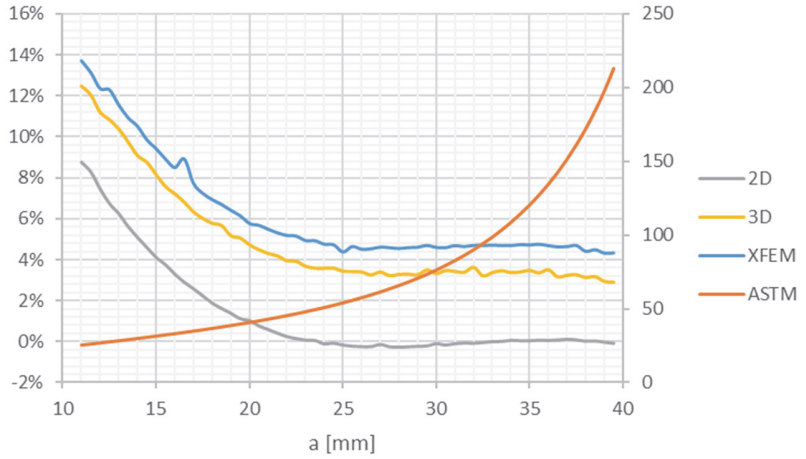

Figure 6: Stress intensity factors vs crack length and obtained differences between ASTM and FEM simulations.

	C	m	Diff. [%]	Diff. [%]
ASTM	1.03E-14	4.06		
2D Contour Integral	8.70E-15	4.15	-16%	2%
3D Contour Integral	6.90E-15	4.17	-33%	3%
3D XFEM	7.00E-15	4.15	-32%	2%

Table 5: Paris Law parameters determined for each type of FEM simulation, for the HAZ material.

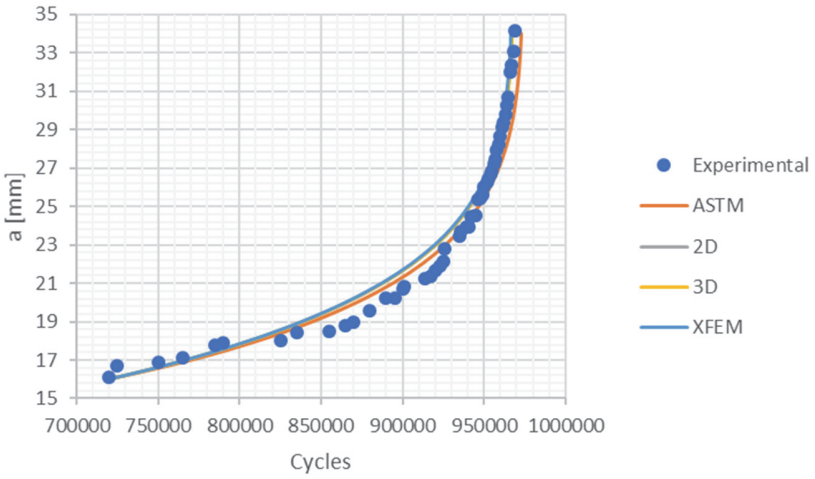

Figure 7: Experimental fatigue crack growth on the HAZ vs FEM simulations using different models.

Fatigue crack growth on a CT specimen containing a longitudinal weld

When considering welded specimens, Zong et al. [23] have also used this technique to calculate fatigue crack propagation. Unlike the second case presented in this paper, Zong et al. [23] did not considered the full three-dimensional geometry of the longitudinal weld. When considering the weld geometry, the specimen will be subjected to a mixed mode loading, as K_{II} will no longer be zero. This means that the MTS criterion will predict crack kinking, according to Eqn. (2). As one can see in Fig. 8 a), the algorithm is accurately predicting the crack deflection. As mentioned the 2D and 3D have different geometries. The 2D is just an approximation, and in fact contains more material in the simulated weld. Therefore, one can see the 2D model predicts a higher crack deflection. The 3D models predicted very close results, with the crack deflected by 1 mm over a 40 mm length crack, while the 2D models predicted a 2 mm deflection for the same crack length. The

different modeled geometry is also responsible for the different predicted fatigue life, Fig. 8 b), as the SIF for mode I are lower on the 2D model, resulting in a lower crack driving force.

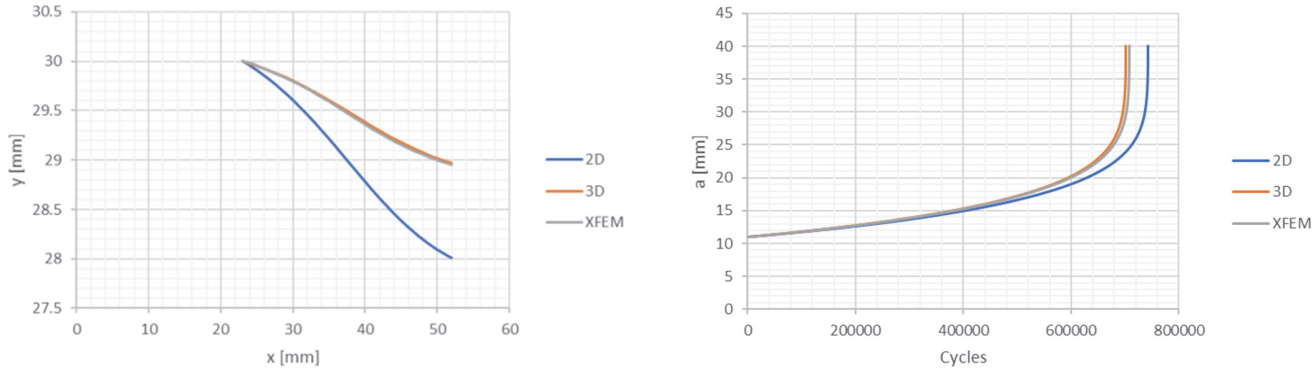

Figure 8: a) Fatigue crack growth paths, b) Crack propagation curves on the HAZ of a specimen with a longitudinal crack, using different FEM simulation models.

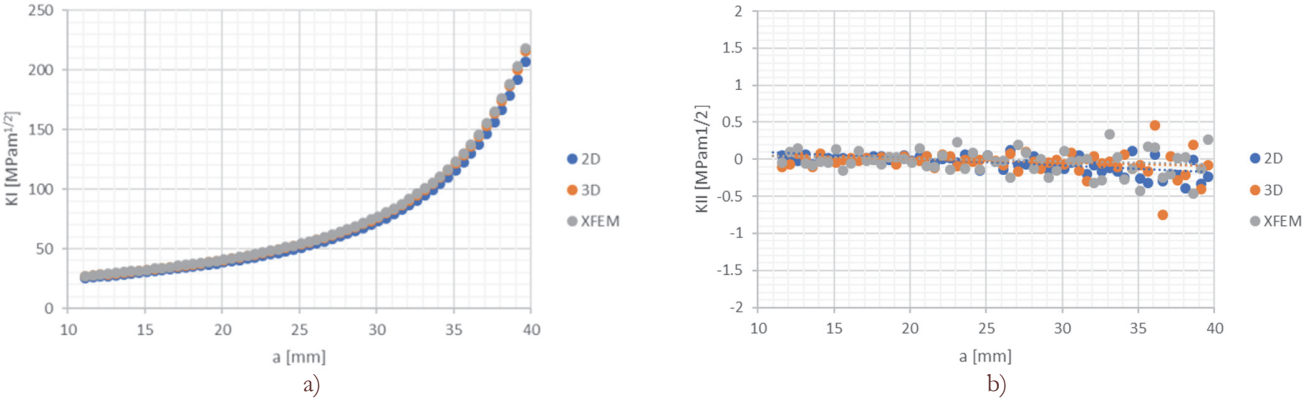

Figure 9: Stress intensity factors using different FEM simulation models, a) mode I, b) mode II.

Fig. 9 show the evolution of K_I and K_{II} as the crack is propagating. In Fig. 9 a) one can see the evolution of K_I, as expected the SIF increases as the crack length increases. While in Fig. 9 b) one can see the evolution of K_{II}, for small cracks K_{II} is almost zero, but as the crack length increases the absolute value of K_{II} will increase, as the crack is propagating in mixed mode. As the crack propagation direction is calculated from the previous increment values of K_I and K_{II} according to Eqn. (2), the crack deflecting is in this case influenced by the evolution of K_{II}. Fig. 9 b) show the existence of some numerical noise, as the value of K_{II} can change from positive from negative, from one increment to the other. Shi et al. [13] have also reported this behavior. The 2D model is the one with less numerical noise, while the 3D model using the contour integral technique show small noise for smaller cracks, but a larger noise for larger cracks. As mentioned by Shi et al. [13], the numerical noise can be reduced by using a smaller crack length increment. In our case the increment used was 0.5 mm for all models. Shi et al. [13] reported that the best results were obtained with a fixed crack length increment of 0.3 mm. The difference, when using a 1 mm increment, is not significant. Fig. 10 show the evolution of the crack resulting deflection angle, as calculated by the MTS criterion and Eqn. (2). As mentioned initially the crack propagates in mode I, as the deflection angle is low. But as the crack grows and the value of K_{II} increase, the deflection angle also increases, and the crack propagates in mixed mode. The increase is higher for the 2D model, justifying the obtained results. For bigger cracks, as the value of K_I increases, the deflection angle decreases, and the crack will again behave as in pure mode I.

As a final remark, as mentioned by Nasri et al. [21], if the crack deflection increases, the crack propagation will be delayed. Therefore the 6% increase in the fatigue life for the 2D model, is also justified by the increase crack deflection offer by this model.

Crack deflection can be seen in Fig. 11. Here the 3D contour integral model is shown for the normal CT specimen (Fig. 11 a)) and for the longitudinal welded specimen (Fig. 11 b)). It is possible to see the crack propagating in the horizontal direction for the normal specimen, while the crack is deflected in the welded specimen. Fig. 12 show different snapshots

of the crack propagation simulation on the 3D contour integral model containing a longitudinal weld, representing the crack opening process and the corresponding stress distribution fields.

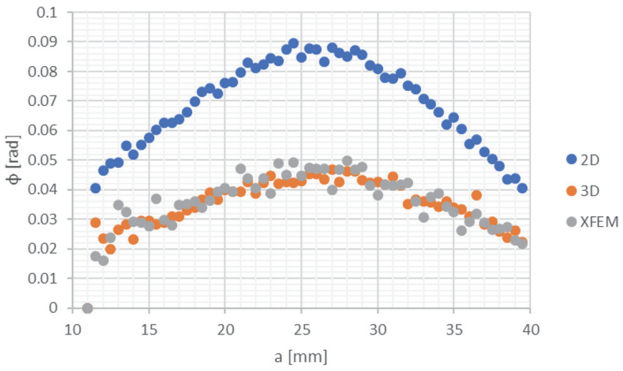

Figure 10: Crack deflection angle, calculated using the previous increment values of K_I and K_{II}.

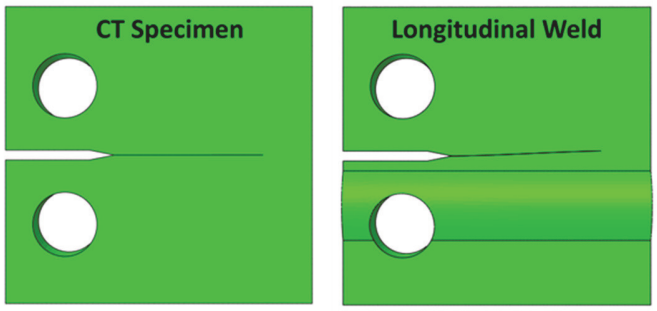

Figure 11: Crack propagation paths on both specimens, without and with a longitudinal weld.

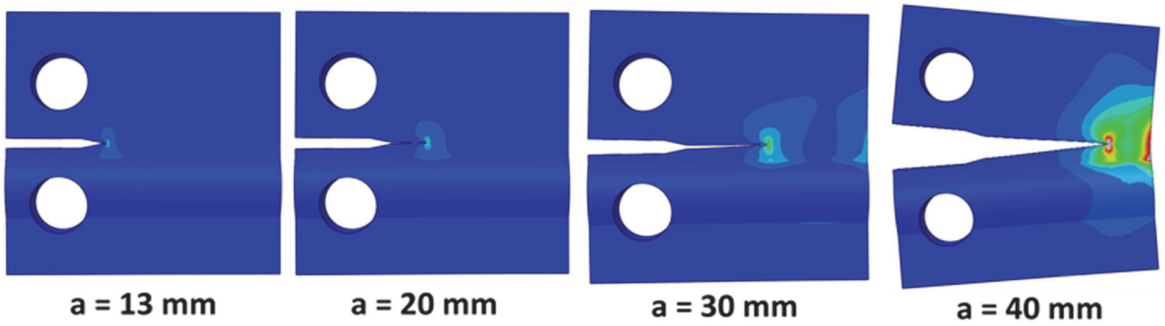

Figure 12: Crack opening and stress distribution field on a CT specimen containing a longitudinal weld, for different crack lengths.

Conclusions

CT specimens of welded high strength TMCP steel, supplied under the requirements of S700MC, were fatigue tested in agreement with the ASTM E647 standard. The Fatigue crack growth behavior of the HAZ was obtained. In order to predict the fatigue performance of welded components, made out of this or other materials, an algorithm for automatic fatigue crack propagation was developed. The algorithm is open and modular, it can work with different FEM solvers and different techniques to extract fracture mechanics parameters. It is also possible to use different crack propagation criteria. Using ABAQUS as the FEM solver, 2D and 3D models, the contour integral and the XFEM techniques, normal and welded CT specimens were simulated. The algorithm accurately predicts crack propagation on the normal CT specimen, and different models can be used to determine the Paris Law material parameters. The algorithm can also be used to predict mixed mode crack propagation, on the longitudinal welded specimens. The modeled

weld geometry deflects the crack, and it was possible to use the MTS criterion to predict the crack propagating direction along the fatigue crack growth. When using 2D models, the extracted SIF showed less numerical noise in the simulation, but the recreated geometry is only an approximation of the real geometry. Therefore, one must recommend the use of 3D models when possible.

REFERENCES

[1] Maier, B., Guster, C., Tichy, R. and Ecker, W. (2013). Influence of different microstructures of the welding zone on the fatigue crack growth behaviour of HSLA steels, , pp. 1–7.

[2] Wang, Q., Liu, X., Wang, W., Yang, C., Xiong, X. and Fang, H. (2017). Mixed mode fatigue crack growth behavior of Ni-Cr-Mo-V high strength steel weldments, Int. J. Fatigue, 102, pp. 79–91, DOI: 10.1016/j.ijfatigue.2017.05.001.

[3] Ayatollahi, M.R., Razavi, S.M.J. and Yahya, M.Y. (2015). Mixed mode fatigue crack initiation and growth in a CT specimen repaired by stop hole technique, Eng. Fract. Mech., 145, pp. 115–127. DOI: 10.1016/j.engfracmech.2015.03.027.

[4] Singh, I.V., Mishra, B.K., Bhattacharya, S. and Patil, R.U. (2012). The numerical simulation of fatigue crack growth using extended finite element method, Int. J. Fatigue, 36(1), pp. 109–119. DOI: 10.1016/j.ijfatigue.2011.08.010.

[5] DIN. (2013). EN 10149-2: Hot rolled flat products made of high yield strength steels for cold forming - Part 2: Technical delivery conditions for thermomechanically rolled steels.

[6] RautaruukkiCorporation. RautaruukkiCorporation.(2014). Hot-Rolled Steel Sheets, Plates and Coils: Welding.

[7] ASTM International. (2002). ASTM E466-96: Standard Practice for Conducting Force Controlled Constant Amplitude Axial.

[8] ASTM International. (2001). ASTM E647-00: Standard Test Method for Measurement of Fatigue Crack Growth Rates.

[9] Baptista, R., Santos, T., Marques, J., Guedes, M. and Infante, V. (2018). Fatigue behavior and microstructural characterization of a high strength steel for welded railway rails, Int. J. Fatigue, 117(January), pp. 1–8. DOI: 10.1016/j.ijfatigue.2018.07.032.

[10] Dhondt, G. (2014). Application of the Finite Element Method to mixed-mode cyclic crack propagation calculations in specimens, Int. J. Fatigue, 58, pp. 2–11, DOI: 10.1016/j.ijfatigue.2013.05.001.

[11] Paris, P. and Erdogan, F. (1963). A critical analysis of crack propagation laws, J. Basic Eng., 85(4), pp. 528–533. DOI: 10.1115/1.3656900.

[12] Rabold, F. and Kuna, M. (2014). Automated Finite Element Simulation of Fatigue Crack Growth in Three-dimensional Structures with the Software System ProCrack, Procedia Mater. Sci., 3, pp. 1099–1104. DOI: 10.1016/j.mspro.2014.06.179.

[13] Shi, J., Chopp, D., Lua, J., Sukumar, N. and Belytschko, T. (2010). Abaqus implementation of extended finite element method using a level set representation for three-dimensional fatigue crack growth and life predictions, Eng. Fract. Mech., 77(14), pp. 2840–2863. DOI: 10.1016/j.engfracmech.2010.06.009.

[14] Erdogan, F. and Sih, G.C. (1963). On the Crack Extension in Plates Under Plane Loading and Transverse Shear, J. Basic Eng., 85(4), pp. 519. DOI: 10.1115/1.3656897.

[15] Blažić, M., Maksimović, S., Petrović, Z., Vasović, I. and Turnić, D. (2014). Determination of fatigue crack growth trajectory and residual life under mixed modes, Stroj. Vestnik/Journal Mech. Eng., 60(4), pp. 250–254. DOI: 10.5545/sv-jme.2013.1354.

[16] Fajdiga, G. (2015). Determining a kink angle of a crack in mixed mode fracture using maximum energy release rate , SED and MTS criteria, J. Multidiscip. Eng. Sci. Technol., 2(1), pp. 356–362.

[17] Yang, Y. and Vormwald, M. (2017). Fatigue crack growth simulation under cyclic non-proportional mixed mode loading, Int. J. Fatigue, 102, pp. 37–47. DOI: 10.1016/j.ijfatigue.2017.04.014.

[18] Yu, X., Li, L. and Proust, G. (2017). Fatigue crack growth of aluminium alloy 7075-T651 under proportional and non-proportional mixed mode I and II loads, Eng. Fract. Mech., 174, pp. 155–167. DOI: 10.1016/j.engfracmech.2017.01.008.

[19] Zerres, P. and Vormwald, M. (2014). Review of fatigue crack growth under non-proportional mixed-mode loading, Int. J. Fatigue, 58, pp. 75–83. DOI: 10.1016/j.ijfatigue.2013.04.001.

[20] Tanaka, K. (1974). Fatigue crack propagation from a crack inclined to the cyclic tensile axis, Eng. Fract. Mech., 6(3). DOI: 10.1016/0013-7944(74)90007-1.

[21] Nasri, K. and Zenasni, M. (2017). Fatigue crack growth simulation in coated materials using X-FEM, Comptes Rendus - Mec., 345(4), pp. 271–280. DOI: 10.1016/j.crme.2017.02.005.

[22] Lesiuk, G., Kucharski, P., Correia, J.A.F.O., De Jesus, A.M.P., Rebelo, C. and Simões da Silva, L. (2017). Mixed mode (I+II) fatigue crack growth in puddle iron, Eng. Fract. Mech., 185, pp. 175–192. DOI: 10.1016/j.engfracmech.2017.05.002.

[23] Zong, L., Shi, G. and Wang, Y. (2015). Experimental investigation and numerical simulation on fatigue crack behavior of bridge steel WNQ570 base metal and butt weld, Constr. Build. Mater., 77, pp. 419–429. DOI: 10.1016/j.conbuildmat.2014.12.063.